Structural Analysis of a Novel Integral Tank Concept for Hydrogen Storage Onboard Commercial Aircraft

Oom Ortiz de Montellano, T.; Heidebrecht, A.; Hoogreef, M.F.M.

DOI
10.2514/6.2025-1244

Publication date
2025

Document Version
Final published version

Published in
Proceedings of the AIAA SCITECH 2025 Forum

AIAA SciTech Forum
6-10 January 2025, Orlando, FL
AIAA SCITECH 2025 Forum

10.2514/6.2025-1244

Structural Analysis of a Novel Integral Tank Concept for Hydrogen Storage onboard Commercial Aircraft

Tomas Montellano*, Alexander Heidebrecht†, Maurice F. M. Hoogreef‡
Delft University of Technology, P.O. Box 5058, 2600GB Delft, The Netherlands

Growing concerns about the environmental impact of aviation have (re)sparked interest in hydrogen aircraft as a greener alternative. However, using hydrogen as fuel introduces technological challenges, particularly with regard to on-board storage. Integral tanks, which are part of the aircraft's main structure, seem promising but existing designs show limitations in their integration with the airframe and insulation capabilities. To address these issues, this study proposes a new integral tank concept featuring a double wall architecture with vacuum insulation and outward facing structural reinforcements connecting to the fuselage skin. A parametric sizing method based on finite element analysis is developed to assess the mass of a tank employing this concept and its sensitivities to design choices. Preliminary results point to fuel containment efficiencies consistent with previous designs, with buckling stability identified as the critical design criterion. These findings provide the basis for further research and could be complemented by integrating the developed framework into a complete aircraft design tool.

Nomenclature

Latin Symbols

A	=	Area (m^2)
b	=	Width (m)
E	=	Young's Modulus (GPa)
h	=	Height (m)
I	=	Second moment of area (m^4)
k_t	=	Stress concentration factor (−)
K_σ	=	Buckling stress constant (−)
K_τ	=	Buckling shear constant (−)
L	=	Length (m)
m	=	Mass (kg)
P	=	Pressure (Pa)
r	=	Radius (m)
t	=	Thickness (m)

Greek Symbols

η_{FC}	=	Fuel containment efficiency (−)
η_{grav}	=	Gravimetric efficiency (−)
ν	=	Poisson ratio (−)
ρ	=	Density (kg/m^3)
σ	=	Tensile/compressive stress (MPa)
τ	=	Shear Stress (MPa)

Subscripts

b	=	Buckling
div	=	Tank divider
f	=	Fairing
FC	=	Fuel containment
fr	=	Frame
ins	=	Insulation
i	=	Inner
LH_2	=	Liquid hydrogen
o	=	Outer
sk	=	Skin
str	=	Stringer
tank	=	Tank

I. Introduction

In recent years, increasing awareness about the environmental impact of aviation has renewed the interest in hydrogen aircraft. In a time when conventional aviation is responsible for 3.5% of the net anthropogenic forcing [1], adopting hydrogen as a fuel would eliminate carbon emissions not only during flight, but also during fuel production, provided renewable energy sources are used [2]. For this reason, new projects are gaining traction, choosing hydrogen as a

*MSc graduate, Faculty of Aerospace Engineering
†Post-Doctoral Researcher, Faculty of Aerospace Engineering
‡Assistant Professor, Faculty of Aerospace Engineering, m.f.m.hoogreef@tudelft.nl, AIAA Senior Member

solution to meet the industry's goal of net-zero carbon emissions by 2050 [3]. Perhaps the most prominent is Airbus ZEROe, which aims to bring commercial hydrogen aircraft to the market by 2035*.

However, using hydrogen as fuel presents novel technical challenges. Even in liquid form, hydrogen occupies four times the volume of kerosene, making on-board hydrogen storage the key factor for aircraft usability. While various options have been proposed, such as carrying hydrogen in dedicated fuel pods under the wings, the prevailing consensus for conventional tube-and-wing aircraft is that tank(s) inscribed within the fuselage are the most efficient, reducing the aerodynamic and gravimetric penalties associated with tank integration[4]. In addition, these configurations enable the use of integral tanks, which are argued to have superior performance [5, 6]. In contrast to non-integral tanks which are independent "containers", the structure of integral tanks is integrated with the airframe and carries structural loads. The drawback of an integral tank approach is the added design complexity, as a stiffened structure is required to carry the loads of the primary fuselage structure. Hence, even though the majority of authors acknowledge the theoretical superiority of integral designs, the predominant approach in literature is to consider non-integral tanks [4, 7, 8]. This allows researchers to explore a wide variety of designs and the influence of different parameters, regardless of the precise aircraft for which the tanks are designed. Parameters considered in recent studies include tank geometry [7], dormancy time [9] and venting pressure [10].

In the few cases where integral tanks have been considered for their advantages, sizing methods are mostly limited to pressure vessel calculations, and few details are given on how the tank is connected to the aircraft structure [6, 11, 12]. The studies by Brewer [13] and Gomez and Smith [14] are notable exceptions where the sizing of the stiffening structure is explicitly addressed .

Under NASA sponsorship, Brewer proposed an integral tank design consisting of a single stiffened wall covered with polyurethane foam insulation and connected to the fuselage airframe by a a truss-like structure made of boron-reinforced fiberglass tubes. Brewer achieved a mass saving of approximately two tons over a non-integral design by applying this concept to a 400-passenger long-range aircraft[13]. However, the complexity of the truss system discouraged further research or a transition to practical applications. In a more recent study, Gomez and Smith [14] proposed inner insulation to simplify the connection between the stiffened tank structure and the adjacent airframe. However, issues with hydrogen and oxygen permeation into the insulation pores and foam embrittlement raise concerns over the feasibility and durability of this solution.

The previous discussion shows that existing integral tank concepts rely on single wall designs, compromising the integration with the airframe or the insulation capabilities of the tank. Moreover, they are largely confined to the specific aircraft under investigation.

In this research, a new concept with a double-wall construction, with outward-facing reinforcements and vacuum insulation is proposed to address these issues. The inner wall contains the hydrogen and the outer wall physically protects the insulation and limits the permeation of air into the insulation. The space between both walls is evacuated in order to remove both oxygen and hydrogen permeating into the insulation layer, and to enable the use of vacuum-assisted insulation[15]. The stiffeners required by the outer wall are installed on the outside of the tank. This avoids interference with the insulation and makes the wall structure easier to inspect or repair. This in turn makes it easier to integrate the outer wall as part of the load-carrying structure of the aircraft fuselage, since the mechanical load does not need to pass through the insulation layer. The outward-facing stiffeners and reinforcements connect to the aerodynamic skin of the aircraft fuselage. The space between the outer tank wall and the skin allows for passing cables and piping without increasing the fuselage cross-section.

The primary goal of this study is to assess how the structural mass and tank size of such an integral, double-walled tank compares to existing concepts.

A sizing methodology based on a parametric framework is developed and follows a finite element (FE) approach. Rather than a concrete design, this study aims to establish trends and guidelines that can be applied to the first generation of hydrogen aircraft, motivating further research and contributing to an earlier adoption of this technology. Although future aircraft concepts such as Airbus' Blended Wing Body (BWB) can be designed to provide additional volume for hydrogen storage, it is expected that early hydrogen aircraft will use conventional tube-and-wing aircraft, and therefore, this study is limited to conventional tube-and-wing configurations. The following section describes the new concept proposed in this research. Then, section III explains the methodology used to develop the framework. Important results are presented and discussed in section V. Finally, the paper closes with a synthesis of the main conclusions along with recommendations for future research.

*Airbus reveals new zero-emission concept aircraft, https://www.airbus.com/en/newsroom/press-releases/2020-09-airbus-reveals-new-zero-emission-concept-aircraft

II. Novel Integral Double-Wall Tank Concept

This section provides a detailed description of the integral tank concept proposed, highlighting the differences to existing designs. It is divided into the tank structure, insulation strategy and wall materials.

A. Tank Structure

Figure 1 shows a schematic representation of the tank design. The double wall architecture allows each vessel to be optimized for its respective function. The inner tank is responsible for holding the hydrogen and the loads associated with fuel containment, while the outer tank connects to the adjacent airframe and carries the loads of the primary structure. The shape of outer wall can be cylindrical without need for cut-outs/channels. The double wall protects the insulation from external influences and air ingress. With the insulation in between, the outer tank structure can be directly connected to the primary airframe avoiding issues with tank contraction/expansion and heat conduction through the structure.

Note that the tank structure utilizes frames and stringers on the outside, contrary to the concepts proposed by Brewer and Gomez. This configuration is not only safer for crash worthiness but also provides the necessary space for systems routing, avoiding the addition of exterior tunnels. A fairing is then attached to the frames to provide a smooth aerodynamic surface. Since it has no structural purposes, a kevlar layer with a thickness of $1.57mm$ and density of $1.304kg/m^3$ is assumed, derived from Brewer et al. [16]. However, a more direct coupling with a traditional load-bearing aircraft skin can also be envisioned. Industry standard fuselage frames and stringers can be used for these structural reinforcements. Inspectability of the fuselage integral structure is also possible thanks to the outward facing reinforcements.

The mechanical connection between the outer and inner vessel is usually referred to as suspension as it handles the dimensional changes of the inner vessel. While a suspension is also represented in 1, a detailed suspension design is beyond the scope of this research at the moment[†].

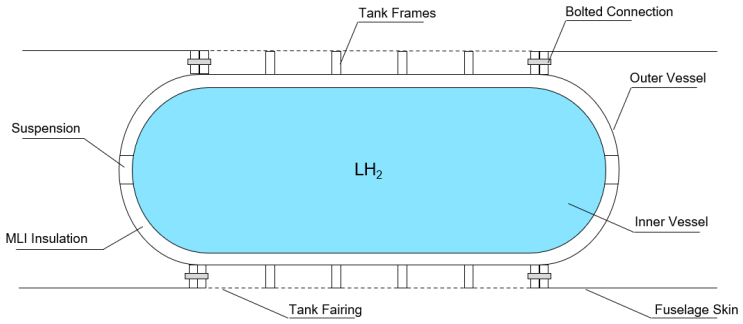

Fig. 1 Integral Tank concept with double wall design and vacuum insulation

B. Insulation and wall architecture

Insulation is required to limit heat flux into the tank, with the temperature difference between the exterior and interior of the tank reaching values of 300°C. As hydrogen boils, the pressure inside the tank rises unless a sufficient amount of hydrogen is removed from the tank. During dormancy times, this may make it necessary to release hydrogen to prevent a structural failure of the tank. This process is known as venting, and the released hydrogen is usually lost unless a complex recovery system is in place [13]. Due to safety and environmental concerns, venting should be avoided whenever possible.

The proposed concept uses multi-layer insulation (MLI) in the space between both walls. MLI consists of alternating layers of reflective shields and low conductivity spacers to minimize the radiative heat transfer through the tank. The radiation shields are often constructed of aluminized or goldized Mylar, while the spacers are typically made of polyester, glass fiber paper, or silk [17]. Since a thermal analysis is outside the scope of this research, MLI properties are extracted from [18], assuming a layer density of 40 layers per centimeter, with a insulation density of $45.0kg/m^3$.

MLI is substantially more efficient when operating at vacuum conditions, achieving thermal conductivity values

[†]Some concepts on such a suspensions exist, e.g. patent US2024116650A1

more than 100 times lower than foam insulation [6, 19]. The higher thermal performance of MLI enables a better control of the tank pressure, allowing the aircraft to stay on ground for extended periods of time. While it is not clear what is the required dormancy time, with values between 2h and 36h found in literature, Huete and Pilidis [9] concludes that venting at the airport should be avoided during early stages of hydrogen aviation due to safety and operational concerns. Given the very low insulation thickness achievable with MLI, dormancy requirements can become easy to meet with only a few millimeters of insulation.

The disadvantage usually pointed to vacuum MLI designs is the requirement to have a double wall construction to hold the vacuum, with researchers claiming a lighter design could be achieved with a single wall design using foam insulation. However, there is an argument to be made that a double wall construction is always required, even with foam insulation. In typical single wall designs, spray on foam insulation (SOFI) is applied on the exterior of the stiffened tank wall. Due to the cryogenic temperatures, air trapped inside the foam may solidify, creating a vacuum that pulls in more air in a phenomenon known as cryopumping [20]. Also, the cold foam becomes brittle and is prone to develop cracks as the aircraft vibrates under normal operation. These effects contributed to the failure of NASA's X-33 prototype and must be avoided by using vacuum or purging the air with an inert gas such as helium, hence requiring a double wall construction. The use of inner insulation such as the one used by Gomez and Smith [14] is expected to worsen this effects, making it unfeasible for aircraft applications. Following this reasoning, Mital et al. [21], who conducted an extensive review on insulation systems, concluded that "a double wall construction with a vacuum-based insulation system may turn out to be an optimum system (. . .)".

A problem for vacuum insulation is the drastic decrease in thermal insulation if vacuum is lost. In this case, the heat entering the tank would require most of the hydrogen to be released in a matter of minutes, which constitutes a serious safety hazard [22]. Nevertheless, such risk can be mitigated by compartmentalizing the vacuum zone, using redundant vacuum pumps, which is a standard practice in the aerospace industry[9], and by adding some amount of redundant insulation layers like aerogel blankets which retain sufficient insulation properties under ambient pressure[15] to prevent catastrophic consequences in such situations.

C. Wall material

Given the demand for extremely light tanks, future designs may use composite materials, with recent prototypes achieving mass savings of up to 75% relative to aluminium designs[‡]. This reduction is particularly relevant for long-range aircraft, which are the most affected by tank mass. A study of particular interest is the research carried by Toray Advance composites (TAC) and the Netherlands Aerospace Center (NLR) in cooperation with partners from the industry and academia, which is developing a tank configuration with an MLI vacuum solution in a double wall configuration[§]. However, since it is not certain to what extent fatigue, inspection and maintenance of composite double-walled tanks would be likely to delay market introduction or require over-sized structures which compromise the benefits, it was decided to focus the work on aluminium, whose properties in this regard are better understood and easier to control.

Given the preliminary nature of this research, the materials were limited to common aluminium alloys used in aviation. A 2219-T851 aluminium alloy was selected for the inner tank, as according to Brewer et al. [16], it provides "ductility at cryogenic temperatures as well as weldability, stress corrosion resistance, high fracture toughness, and resistance to flaw growth.". For the outer tank, 2024-T351 aluminium alloy was adopted based on the data available on its fatigue behavior, derived from Al-Rubaie [23]. The material properties of both alloys are summarized in table 1.

III. Methodology

Although the focus of this research is on tank design, it is crucial to provide a realistic scenario in terms of tank geometry and sizing loads. Therefore, the framework is divided into two parts. The main geometric parameters of the tank are found according to the methods in Section III.A and the loads are determined. Then, the detailed structure of the tank is sized based following the procedures described in Section III.B.

[‡]Hydrogen Central, HyPoint Dramatically Extends Zero-Emission Hydrogen Flight Range With New Ultralight Liquid Hydrogen Fuel Tanks, https://hydrogen-central.com/hypoint-zero-emission-hydrogen-flight-range-ultralight-liquid-hydrogen-fuel-tanks/

[§]Liquid hydrogen composite tanks for civil aviation,https://www.nlr.org/case/case-liquid-hydrogen-composite-tanks-for-civil-aviation/

Table 1 Material properties of 2219-T851 and 2024-T351 aluminium alloys

Property	Symbol	Value	Units
2219-T851			
Density	ρ	2780	kg/m^3
Allowable Hoop stress	σ_H	324	MPa
2024-T351			
Young's Modulus	E	73.1	GPa
Poisson's ratio	ν	0.3	-
Density	ρ	2780	kg/m^3
Tensile Yield stress	σ_y	324	MPa
Compressive buckling constant	K_σ	5.35	-
Shear Buckling Constant	K_τ	4	-

A. Aircraft integration and preliminary tank sizing

Figure 2 illustrates the workflow that was implemented for this research. The first phase (top part of Figure 2) represents a more comprehensive aircraft design tool that performs multidisciplinary analyses to integrate the hydrogen tanks and update the load distribution accordingly. This research builds on previous studies and uses the aircraft geometries generated from such analyses [11] as a platform to calculate the external mechanical loads. While the LH_2 tank mass estimate within the aircraft design loop is preliminary, a reasonable approximation is required since the presence of hydrogen tanks changes the mass distribution of the aircraft, and the wing must be positioned to ensure that control and stability requirements can be met. This affects the stabilizer leverage arm and thus the bending and hear forces borne by the fuselage. Considering the addition of an LH_2 tank to an existing conventional aircraft design is thus likely to lead to unrealistic structural loads.

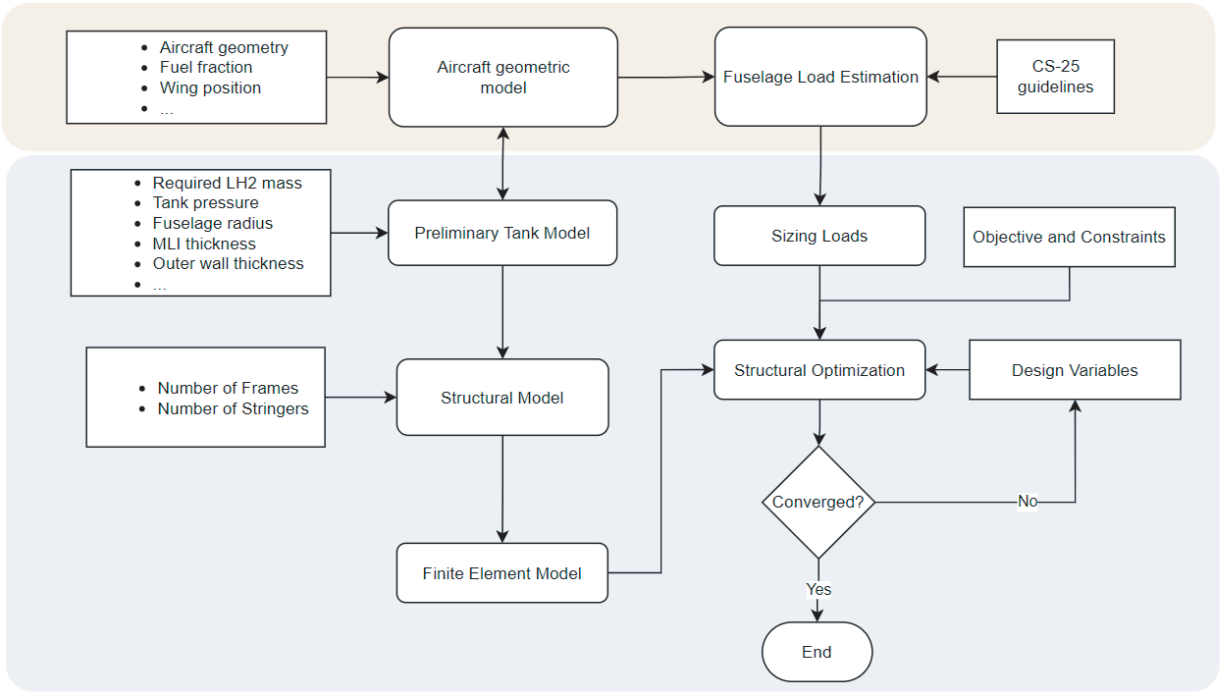

Fig. 2 Aircraft sizing workflow including structural tank sizing.

Based on the generated aircraft model, the mass of individual components is obtained using Class-II weight estimations [24]. Subsequently, the method computes the the loads acting on the fuselage following CS-25 guidelines for fuselage compliance. Then, the internal fuselage loads are determined from beam theory and the loads at the tank location are extracted for the structural analysis. These loads are passed on to the detailed tank sizing (Section III.B.

Two tank layout variants can be created, based on the hydrogen fuel mass required and the fuel fraction between tanks. For a fuel fraction equal to one, a single tank is positioned behind the cabin and the rear pressure bulkhead (hereinafter referred to as aft tank). For fuel fractions lower than unity, an additional tank is positioned in front of the passenger cabin (hereinafter referred to as fwd tank). This option is usually required in larger aircraft to reduce the shift in CG [25]. Since the forward tank separates the cockpit from the cabin, a small passage is required to ensure pilots always have access to the cabin [14, 25] and the passengers can evacuate the aircraft in the time required by aviation standards. For this reason, the forward tank is always non-integral and the detailed tank sizing is limited to the aft tank.

For both variants, the fuselage radius is kept constant (as Onorato et al. [11] found that increasing radius is not generally beneficial) and its length is increased to hold the required volume of the hydrogen tanks, maintaining the passenger capacity of the baseline aircraft. Although a fuselage extension affects airport operations and usually entails an increase in the landing gear mass to ensure the same rear clearance [4], it is not a new approach in the aviation industry. The three configurations (two hydrogen variants and conventional reference) are illustrated in figure 3.

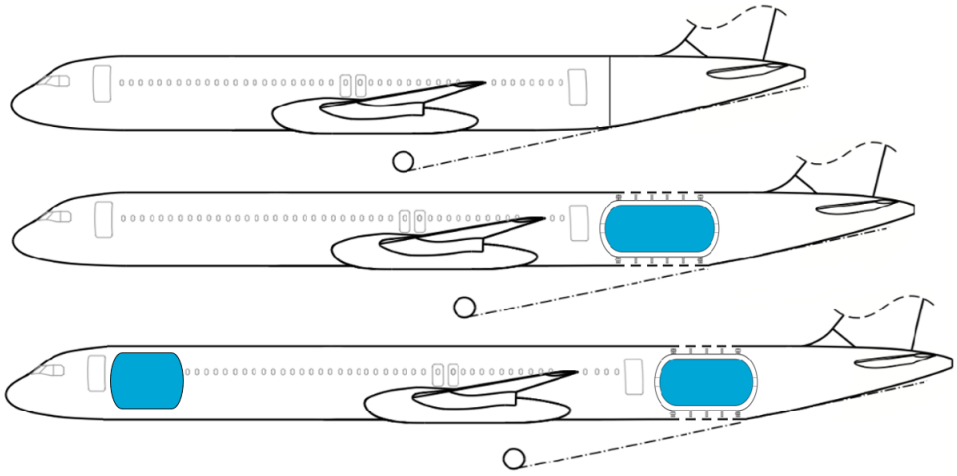

Fig. 3 Baseline aircraft and hydrogen variants, adapted from [26]

1. Preliminary tank sizing

The preliminary sizing of the tank, inside the generation of the aircraft geometric model (top part of Figure 2), is done in four steps. First, the radius of the inner tank is determined based on the values defined for the protective fairing (t_f), frame height(h_{fr}), outer shell thickness(t_{sk_o}), insulation thickness (t_{ins}) and inner shell thickness (t_{sk_i}). Figure 4 gives a visual representation of geometric parameters mentioned. As the outer shell will only be sized in Section III.B, the thickness used here is a guess. The thickness of the inner shell is determined from the hoop stresses caused by the pressurized fuel, according to equation 1.

$$t_{sk} = \frac{Pr}{\sigma_{Hoop}} \tag{1}$$

The tank length is then calculated based on the volume required to carry the specified fuel mass, with preliminary tank sizing based on the work from Onorato [10]. Note that not all of the volume in the tank is occupied by liquid hydrogen. A certain fraction, or "ullage", must be provided to avoid over-pressurization of the tank, especially at the airport during holding times. Commonly suggested values are between 3% and 5%[9]. In addition, volume allowances are required to account for trapped fuel, tank contraction and internal equipment, which add up to 3%, according to Brewer [5]. In total, 8% of the tank volume is deemed unusable.

Only circular cross sections were considered in the current research due to their superiority in handling the pressure loads. However, the tank parameterization also permits the use of elliptical cross-sections, allowing an extension of the

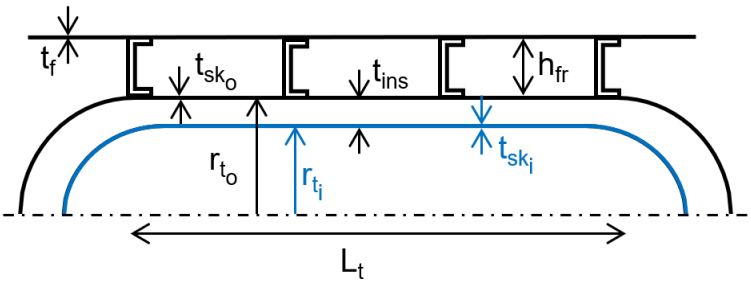

Fig. 4 Tank geometry in preliminary sizing

investigation in this direction. According to Winnefeld, one can expect the thickness of the inner shell to increase up to 5 times [7]. Both spherical and elliptical tank end caps (domes) can be generated at the user's choice.

2. Fuselage Load Estimation

Four main sources of loads are considered, in accordance with CS-25 guidelines for fuselage compliance[14]: weight loads, pressurization loads, aerodynamic loads and ground loads. Using realistic load combinations, internal fuselage loads are determined from beam theory and loads at the tank location for the detailed structural analysis (Section III.B). For all cases, Maximum-Take-Off-Mass (MTOM) is considered in a conservative approach.

- Weight loads: The aircraft is divided into groups and the weight of each group is estimated using Torenbeek class II methods [24]. Contributions specific to the hydrogen aircraft use the relationships defined by Onorato [10]. Based on the aircraft geometry, the weight of all components is applied as a distributed load over the corresponding length, except for the weight of the nose landing gear and pressure bulkheads, which are applied as point loads.
- Pressure loads: The use of a vacuum for thermal insulation subjects the outer shell to an external pressure force. This pressure differential is at its maximum at sea level and at its minimum at the highest flight altitude. This formulation assumes that the tank is located in a non-pressurized section of the fuselage, as this is the safest approach according to Huete and Pilidis [9].
- Aerodynamic loads: Following the methodology in [14], this study considers symmetric pull-up maneuvers and computes the loads at the corners of the flight envelope. The sizing is based on limit loads, which represent the maximum loads that the aircraft is expected to encounter during normal operation. Load factors of 2.5 and -1 are evaluated, as reported by Megson for limit loads [27]. For each case, the balancing tail load is computed after multiplying the weight loads by the respective load factor. To ensure proper sizing of the tank's side panels, lateral cases are also considered, corresponding to loads on the vertical tail caused by lateral gusts or side-slipping flight.
- Ground Loads: In a first approach, only landing cases are considered. In particular, a three-point landing, in which the nose and the main gears contact the runway simultaneously with load factor of 2. A simple rigid body analysis is used to compute the loads, derived from Lomax [28].

Figure 5 shows how the loads described above are applied to the aircraft. The fuselage is assumed to be supported at the wing spars which transmit the vertical forces from the wing and main landing gear. The selected load cases are listed in Table 2.

Table 2 Load cases

Load Case	Description	Load Factor	Mass	Pressure
LC1	Steady flight	1G	MTOM	1.33Δp
LC2	Pull-up manoeuvre	2.5G	MTOM	1.33Δp
LC3	Push-down manoeuvre	-1G	MTOM	1.33Δp
LC4	Lateral gust	1G	MTOM	1.33Δp
LC5	Engine out	1G	MTOM	1.33Δp
LC6	3 Point landing	-2G	MTOM	1.33Δp

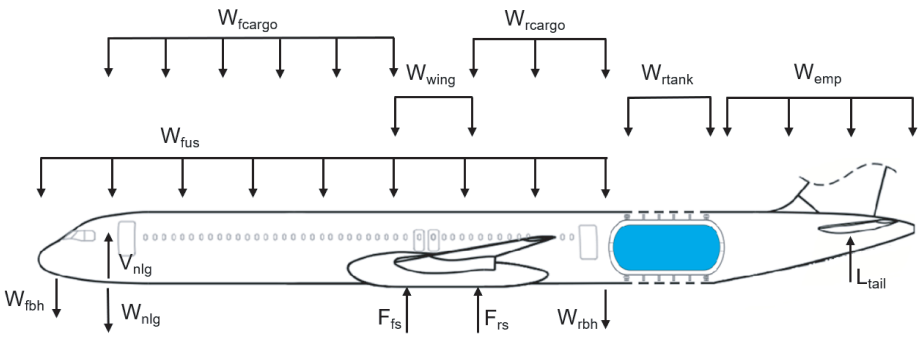

Fig. 5 Forces acting on aircraft, adapted from [29]

B. Detailed Tank Sizing

The second step of the methodology is represented in the top part of Figure 2. It sizes the external stiffened wall of the aft tank to handle the loads obtained from the aircraft design (Section III.A. The detailed tank sizing was implemented as a sub-discipline to the multidisciplinary aircraft design loop, although its output was not integrated into the design loop, due to the computational requirements.

The sizing regards the locations of frames and stringers as constant, and determines the required material thickness of all elements as well as stringer height (see Section III.B.3). To create the structure model, the preliminary tank model is transformed into a structural model by representing all the crucial elements of the tank structure such as the frames and stringers. Next, a mesh is created to discretize the model into individual elements (see Section III.B.2. The optimization problem is then formulated as a structural mass minimization problem. It considers specific design criteria to size the structural elements, which are given as constraints on the strength, buckling stability and fatigue behavior, but does not change the number or locations of frames or stringers. The computational cost associated with this form of structural optimization is considerably less than a full topology optimization and therefore is a suitable choice for this work. The NASTRAN input is automatically generated and the structural mass minimization is performed, using NASTRAN SOL200. [¶] The final result is a structure that meets the design requirements. Further details on the structural model are in Section III.B.1.

To efficiently explore the design space and quickly generate and analyze different structural designs, the process is implemented with a Knowledge Based Engineering (KBE) application, automating repetitive tasks. Among the available tools, the ParaPy platform[‖] was selected for this research project due to its capabilities of building complex models based on the principles of KBE and Object-oriented Programming (OOP), as well as providing meshing tools and an interface to the NASTRAN FEM solver.

1. Structural Model

The structural model of the tank consists of a cylindrical shell, stiffened by stringers, frames and closed by domes. As shown in figure 6, stringers are evenly distributed around the tank, based on the total number of stringers defined by the user. Similarly, the frames are equally spaced based on the number of frames defined, with the first and last frames always positioned at the ends of the cylindrical section of the tank. The cross sectional shape of the stiffeners is also depicted in figure 6. For simplicity, the thickness is assumed to be constant over the flanges of the stiffeners (h), and the height of both stringers is twice their width (b). It is important to note that this work does not explicitly model the connections between the different structural elements.

2. Meshing

The meshing process is entirely automated in ParaPy, to generate a high-quality mesh for different combinations of the input parameters.

Thin structures such as the tank skin are represented by 2-dimensional elements, defined at the mid-surface of the component. This approximation is valid when the thickness of the skin is much smaller than its other dimensions, making

[¶] It is worth noting that NASTRAN uses a gradient-based method that relies on design sensitivities to find the best search direction.

[‖] `https://parapy.nl/`

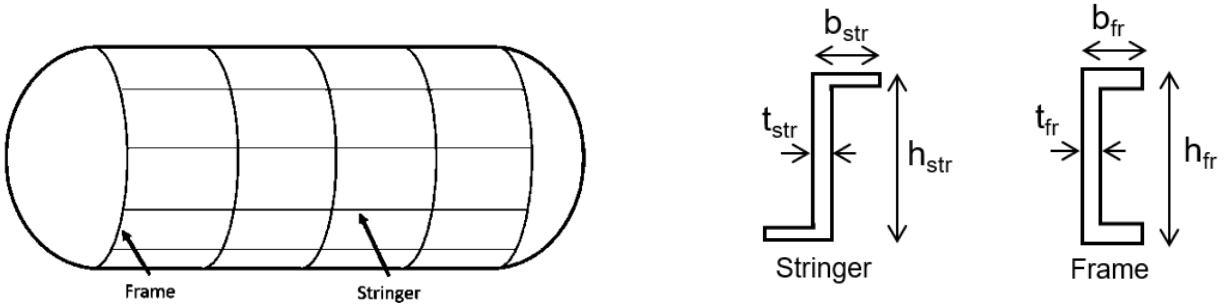

(a) Cylindrical tank with stiffeners, adapted from [30] **(b) Details of stringer and frame**

Fig. 6 Structural tank model

the stress developed in the thickness direction negligible. In particular, NASTRAN shell elements are used, which are capable of capturing both in-plane and bending stresses, based on Kirchhoff theory [31]. The skin is represented with rectangular elements (CQUAD4). Frames and stringers can be represented using 1-dimensional elements; a valid approximation when one dimension (length) is much larger than the other two. To ensure element connectivity, these elements use the same mesh nodes as the skin, and a section offset is introduced to account for the stiffener position relative to the skin. The complete mesh is shown in figure 7.

Since frames and stringers are spaced at constant intervals, all skin fields on the cylindrical shell have the same size. The shell mesh resolution is defined by specifying the number of elements between adjacent frames and stringers, with the former being chosen such that the resulting mesh elements have an aspect ratio close to 1. This results in a shell mesh with constant element size on the cylindrical part. The beam elements representing frames and stringers are subdivided into equal-length segments such that they match the element size and location of the shell mesh.

The computational cost thus depends on the number of elements per skin field, and was minimized by finding the minimum number of elements that still represents the geometry and produces acceptably accurate results. This number was determined after performing a mesh convergence study, which is described in SectionIV.B.

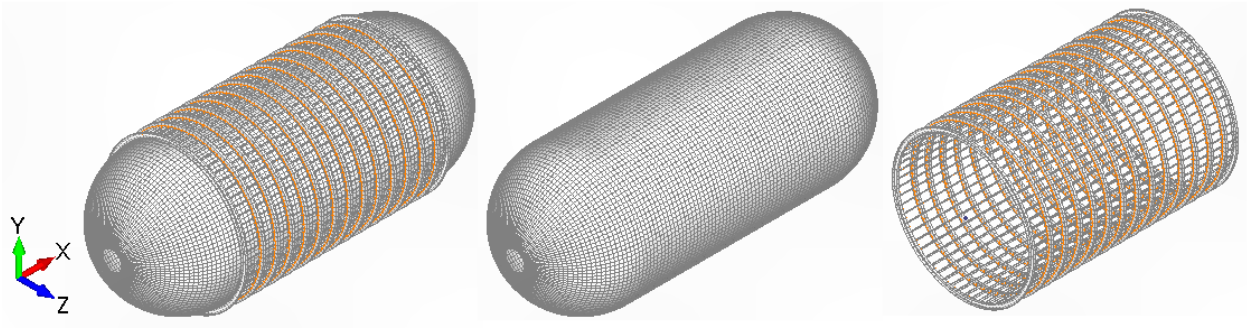

Fig. 7 Complete FE model

The external pressure load is applied at the center of each skin element, pointing inwards. The bending moment and shear force from the fuselage are transformed into equivalent nodal loads and applied at both ends of the tank's cylindrical section. The bending moment is applied through axial loads with a magnitude proportional to the distance to the neutral line, while the shear flow over the cross section is represented by circumferential loads. For a detailed explanation of this method, refer to [32].

The model is constrained using the inertia relief option in NASTRAN, which is commonly used in aerospace to analyze objects in flight. This option uses the structure's inertia to create a static equilibrium, allowing the model to be solved and avoiding unrealistic stress concentrations caused by typical boundary conditions if the sums of all forces and moments do not exactly equal zero, due to imperfect numerical accuracy. The validity of this approach was tested in section IV.

3. Design variables

There are three main types of structural optimizations used in aircraft design: topology, shape and size optimization. In this work, only the latter is applied due its lower computational cost, following the same approach as Nanninga[33]. Hence, the parameters that define the shape and topology of the structural model are fixed, including the tank length, radius and number of stiffeners. Based on this layout, geometric design variables are defined to have control over the size and thickness of the individual components. In addition, a simplified topology study is performed by means of a Design of Experiments (DOE) to obtain the tank shape and stiffener layout that minimizes structural mass.

Table 3 summarizes the sizing variables, including their upper and lower bounds which define the the design space. The lower bounds are based on manufacturing limits, while the upper bounds ensure a wide design space without producing unrealistic designs. The skin thickness is divided into three sections (top and bottom, sides, and domes) to allow independent control over each section.

Table 3 Definition of the design space

Design Variable	Lower bound	Upper bound	Unit
Skin Thickness (t_{sk})	0.5	15	mm
Stringer Thickness (t_{str})	0.5	10	mm
Stringer Height (h_{str})	20	120	mm
Frame Thickness (t_{fr})	0.5	15	mm

4. Sizing Objective and Constraints

The mass of the external shell structure is selected as the objective function of the optimization and it is the sum of the individual masses in the model. Each mass is calculated from the element volume and the defined material density.

$$m_{struct} = m_{skin} + m_{stringers} + m_{frames} \tag{2}$$

The constraints on the design result from the design criteria selected for this method. All constraints are subject to a safety factor (SF) of 1.5, except for skin buckling, which is expected to occur at limit load. The strength criteria is imposed by comparing the stress in each element against the material yield stress (σ_y), resulting in constraints for the skin panels and the stiffeners:

$$R_{yield} = \frac{\sigma}{\sigma_y SF} < 1 \tag{3}$$

Where σ is the stress measured on the finite element model for each element. The Von Mises stresses are used for the skin panels and the maximum section stress is retrieved for each stiffener element.

Skin instability due to buckling is controlled by limiting the combined compressive and shear stresses on the skin panels according to equation 4.

$$R_{sk_b} = \frac{\sigma}{\sigma_{b_{crit}}} + \frac{\tau}{\tau_{b_{crit}}} < 1 \tag{4}$$

Here, the critical buckling stresses are calculated following simple shell buckling formulae, assuming simply-supported edges and considering the distance between stringers as the panel width.

$$\sigma_{b_{crit}} = K_\sigma \frac{\pi^2 E}{12(1-\nu^2)} (\frac{t_{sk}}{b_{sk}})^2 \tag{5}$$

$$\tau_{b_{crit}} = K_\tau \frac{\pi^2 E}{12(1-\nu^2)} (\frac{t_{sk}}{b_{sk}})^2 \tag{6}$$

Above a certain stress level, the skin will start to buckle and becomes ineffective at carrying additional load. At this condition, the stringers behave as independent columns, with their length determined by the distance between frames. The load at which stringers buckle is calculated according to the formula by Euler, given in equation 7. The constraint function for stringer column buckling is defined in Equation 8.

$$\sigma_{Euler} = \frac{\pi I_{xx} E}{L_{fr}^2 A} \tag{7}$$

$$R_{str_b} = \frac{\sigma}{\sigma_{Euler} SF} < 1 \tag{8}$$

Finally, a constraint on fatigue is imposed to prevent structural failure under cyclic loads.

$$R_{Fat} = \frac{\sigma}{\sigma_{Fat} SF} < 1 \tag{9}$$

Here, σ_{Fat} is calculated according to the exceedance frequency model proposed by NLR [34], using Equation 10 (a substitution of the general fatigue life model described by [23]). In this model, the stress levels at 1g flight are taken as reference and scaling factors are empirically determined for each exceedance frequency, considering 40000 flights of 1.5h. As an example, the scaling factor for 100 exceedances is 1.215, meaning that 100 times per 60000 flight hours, the stress on the structure exceeds the "steady flight" stress by a factor of 1.215. 60000 flight hours matches Airbus' Design Service Goal (DSG) for the A320 and A330 families and is the value used for design and validation of the maintenance programme [35]. In a conservative approach, the stress was calculated for each exceedance frequency in [34] and the minimum was taken for the fatigue constraint.

$$\sigma_{Fat} = \frac{(N \cdot 10^{-A})^{-\frac{1}{B}} + D}{k_t^E (2 - \frac{2}{Scale})^C} \tag{10}$$

The factors A to E depend on the material characteristics and were retrieved from the study by Al-Rubaie [23]. k_t is a stress concentration factor to account for geometric discontinuities in the structure, such as holes or keyways, which can lead to crack initiation or propagation. A factor of 4.5 was assumed with a sensitivity study performed in section V. The scale factor depends on the exceedance frequency and is specified in [34], ranging from 2.6 for a frequency in the order of 10^1 to 1.247 for 10^6.

C. Fuel Containment Efficiency

The primary goal of this study is to evaluate the feasibility of the new proposed concept by comparing its performance against other designs. Given the importance of mass in aircraft design, a mass based evaluation parameter seems an appropriate choice. The widely accepted metric to measure tank performance is the gravimetric efficiency of the tank, as defined in (11).

$$\eta_{grav_{struct}} = \frac{m_{LH_2}}{m_{LH_2} + m_{tank}} \tag{11}$$

Where m_{LH_2} is the hydrogen fuel mass and m_{tank} is the mass of the empty tank.

However, a review of current literature showed that a large spectrum of gravimetric efficiencies ranging from 0.25 to 0.85 can be found [36], which is attributed to the lack of consistency in defining the terms in (11), e.g. whether m_{LH_2} refers only to usable hydrogen, and whether residual hydrogen and fuel systems are included in m_{tank}. To provide clarity in the mass estimation, the definition in (12) is used in this research, where m_{LH_2} includes unused fuel and possible vented fuel, and m_{FC} concerns only the mass related to the fuel containment (FC). Hence, we define a "fuel containment efficiency" relating the (gross) hydrogen mass to the tank structural mass as follows:

$$\eta_{FC} = \frac{m_{LH_2}}{m_{LH_2} + m_{FC}} \tag{12}$$

$$m_{FC} = 1.08 \left(m_{fairing} + m_{wall_i} + m_{wall_o} + m_{ins} + m_{div} \right) \tag{13}$$

The fuel containment mass calculated by this method includes the mass of the external stiffened wall m_{wall_o} (as defined in (2)), the mass of the insulation m_{ins}, the mass of the inner wall m_{wall_i}, tank dividers m_{div} (assuming similar mass as for the end caps as their construction is similar, estimated at 100kg for the aircraft considered according to Onorato [10]) and the mass of the fairing $m_{fairing}$ (i.e. local section of fuselage skin attached to outer wall reinforcements). In addition, Brewer [5] suggests that an allowance of 8% should be used to account for manufacturing tolerances, joints and supports required for fuel related operating systems such as pumps, valves and sensors. However, it does not include the mass of the fuel system or the connection between the inner and outer shells. This should always be noted when using the results from this study.

IV. Verification

Before extracting the results, various steps were taken to verify and validate the framework.

A. Load Application

The structural response of the model to the selected loads is dependent on how the loads are applied. Therefore, it is critical to verify not only that the equivalent loads produce the correct bending moment and shear force but also that the structure responds in the expected manner. To this end, an aluminum test cylinder stiffened with C-frames and Z-stringers was used, with dimensions and loads adapted from a structural fuselage study and summarized in Table 4. Note that the internal pressure is specified as negative to reflect the external pressure acting on the tank wall.

Table 4 Dimensions and loads of the aluminium test tank, adapted from [32]

Parameter	Value	Unit
Tank length	970	mm
Tank radius	250	mm
Skin thickness	1.0	mm
Stringer thickness	1.0	mm
Stringer height	20	mm
String width	15	mm
Frame thickness	1.2	mm
Frame height	40	mm
Frame width	20	mm
Pressure	55000	Pa
Bending moment	4000	Nm
Shear force	600	N

Figure 8 shows the difference between the desired bending moment and shear force and the numerically-integrated nodal loads. The errors relative to the desired load are well below 10^{-8}, regardless of the number of stringers.

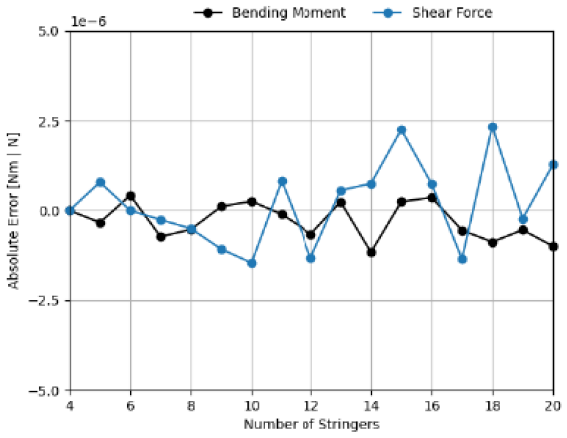

Fig. 8 Load application errors

Figure 9a displays the minor principle stresses on the skin when only external pressure is applied. It is noteworthy that the skin panels between the stiffening elements are under compression and therefore susceptible to failure due to buckling. It can also be seen how the stringers and frames alleviate the compressive stresses on the skin, which is in line with the mathematical relations defined earlier in this research. Finally, the domes appear to have a good resistance to the external pressure, even though they are not stiffened.

Figure 9b shows the longitudinal stresses on the skin under a positive bending moment about the 'Y' axis. As expected, the highest stresses are found on the top and bottom; panels at the former side being under compression and the latter under tension. On the contrary, the stresses on the side panels are low, since they are close to the neutral line of the structure.

The same observation can be made for the stiffeners, as depicted in Figure 9c. For the same reasons, moments about the 'X' axis due to lateral load cases put the side panels under tension and compression, with minimal impact on the top and bottom panels.

The structural response under shear loads was also evaluated. Figure 9d shows the distribution of shear stresses on the skin under a positive shear load in the vertical direction. As anticipated, the shear stresses are coherent with the shear flow on the section, which has a sinusoidal shape.

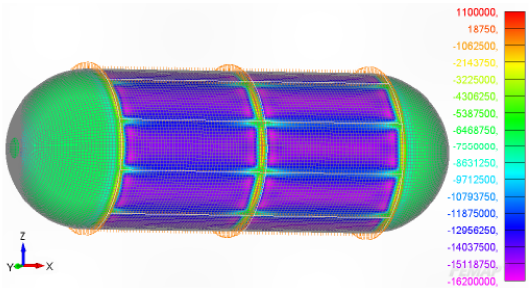

(a) Mean stresses on tank skin under external pressure load

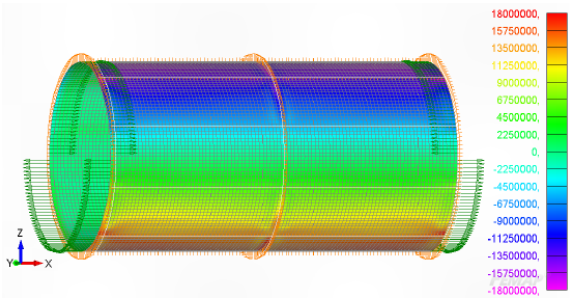

(b) Longitudinal stresses on the skin under a positive bending moment

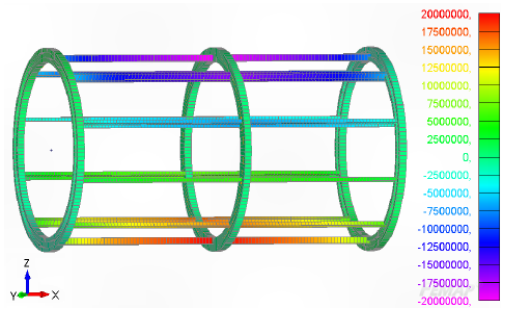

(c) Stresses on the stiffeners under a positive bending moment

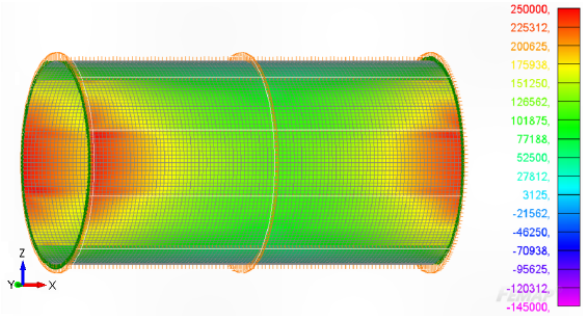

(d) Shear stress on the skin under a positive shear force.

Fig. 9 Verification of load applications

B. Mesh Convergence

To evaluate the impact of mesh density on the results, the sizing procedure was repeated for different meshes, with varying number of elements between stringers. Figure 10 depicts the results obtained, along with the coarsest and finest meshes considered. It is evident that after a certain number of elements, the computational time increases significantly more than the accuracy, which is expressed as the mass difference from the results obtained with the finest mesh.

Based on these results, a mesh with 8 elements between stringers was chosen for the analyses in this research. When compared to the solution obtained with 10 elements between stringers, it is 6.75% faster and converges to a mass 0.04% lower.

C. Pressure Vessel case

Finally, a simple case with a known analytical solution was selected to test the optimizer. The case involved a cylindrical shell with a radius of 0.5mand a length of 2m that was subjected to an inner pressure of 100kPa. The objective was to optimize the shell for minimum mass while limiting the hoop stresses to 85MPa.

This case was also used to compare the boundary conditions of the FE model, testing both a solution with inertia relief and one with the nodes on one end of the shell fixed in all degrees of freedom. The first case produced a skin

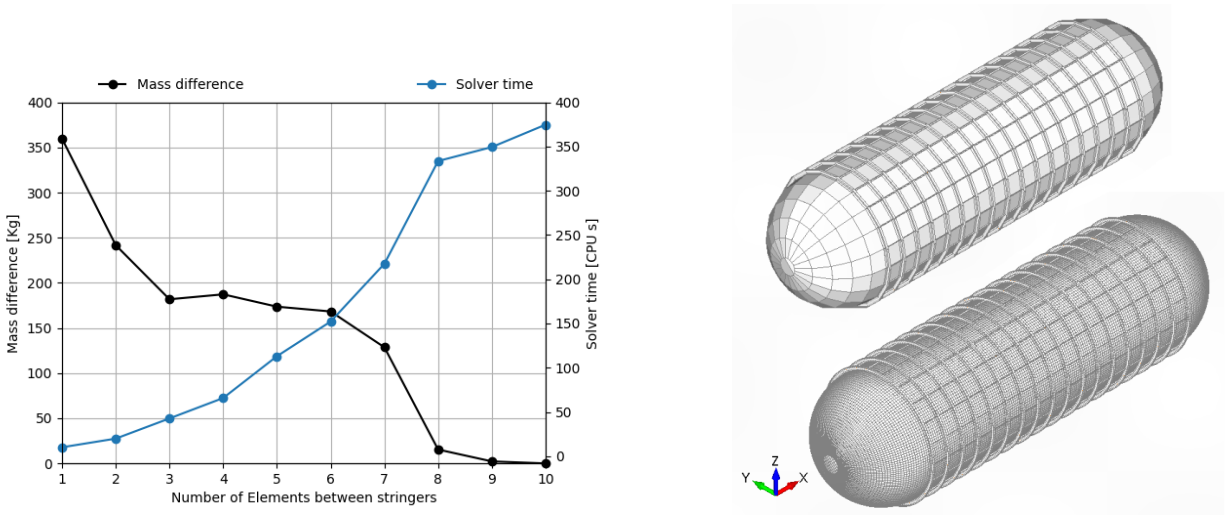

(a) Mesh convergence plot **(b) Meshes with 3360 and 295200 elements**

Fig. 10 Mesh convergence study

thickness of 0.59mm, which matches the analytical solution. However, the constrained case resulted in a skin thickness of 0.62mm, exceeding the exact value by 5.1%. Figure 11 shows the distribution of hoop stresses on the models. It also reveals the unrealistic stress concentration near the boundary condition that leads to the error in the results. This confirms the choice to use the inertia relief boundary condition for all further analyses.

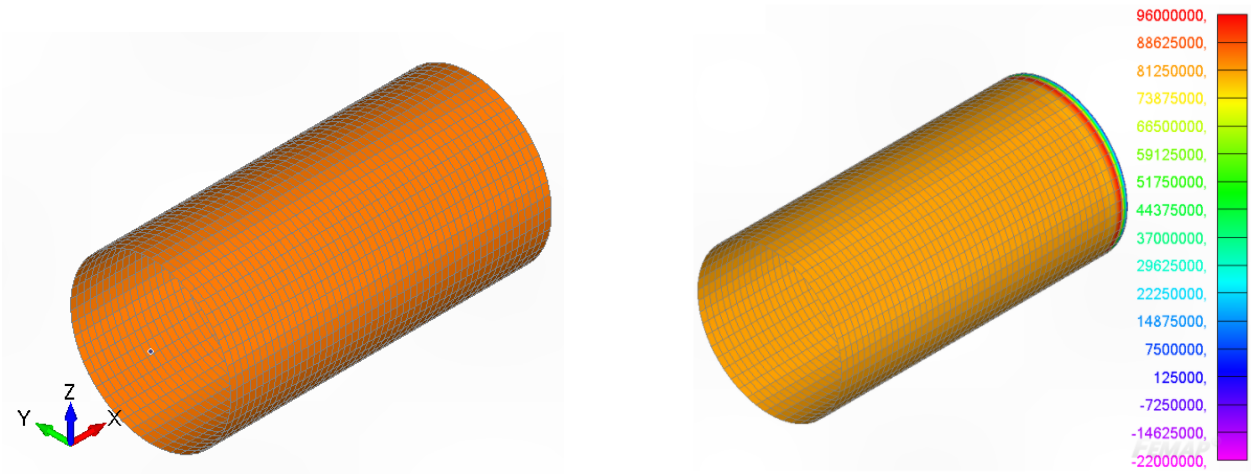

(a) Inertia Relief **(b) aft end fixed**

Fig. 11 Contour of circumferential (hoop) stresses on the FE model

V. Analysis and Results

The method described in this research was used to size the structure of an aft tank integrated into an A320-200. In particular, the hydrogen aircraft versions generated by Onorato et al. [11] were used, as they already reflect the required changes at aircraft level to integrate the hydrogen tank(s) and therefore provide a realistic sizing scenario.

Three aircraft geometry models were built based on available data. First, a baseline model recreates the reference aircraft, following data from Airbus. The variant used is the WV0055 with a MTOM of 79.0, a OEM of 45.0t and 150 passengers distributed over two classes. Then, two hydrogen variants are built based on data from Onorato et al.

[11]. The first has a single aft tank behind the passenger cabin, while the second has both an aft and a forward tank. Both aft tanks have an integral structure, while the forward tank is non-integral. These variants correspond to aircraft SMR-LH_2-b and SMR-LH_2-e in Onorato et al. [11], updated to represent the tank design proposed in the present article. The aircraft were updated accordingly to have a consistent mass breakdown.

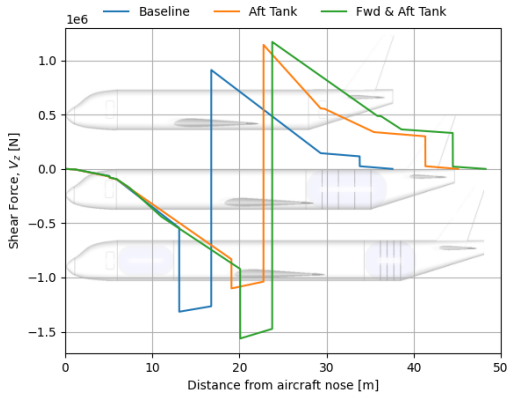

(a) Shear Force due to 2.5g pull-up

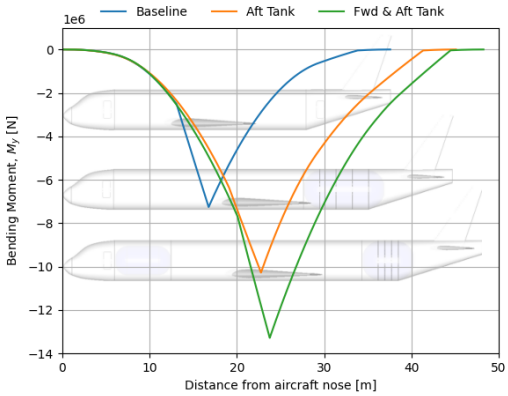

(b) Bending Moment due to 2.5g pull-up

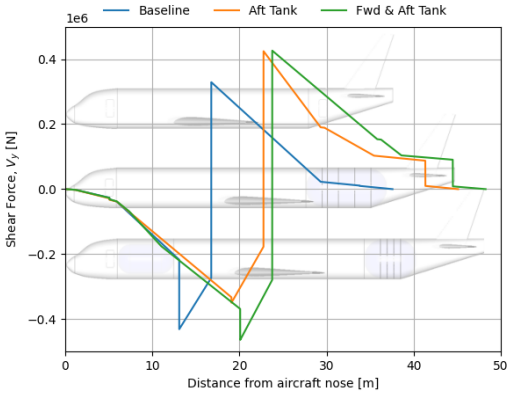

(c) Shear force due to engine-out

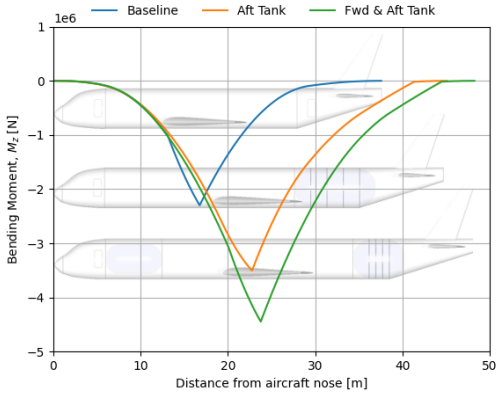

(d) Bending Moment due to engine-out

Fig. 12 Shear force and bending moment diagrams for the baseline aircraft and hydrogen variants

Based on the aircraft models, internal fuselage loads in the form of shear force and bending moment were determined for each of the load cases defined in Table 2. Figure 12 highlights the maximum values obtained, corresponding to symmetric maneuvers with a load factor of 2.5g and side-slipping flights in an engine out condition. The graphs clearly indicate that the fuselage of the hydrogen aircraft is subject to higher loads, particularly at the wing position, as the wing loses the bending relief from the kerosene fuel. Moreover, there is an increase in bending moment and shear force as the length of the fuselage increases. The loads required for the sizing of the tank structure are retrieved at the location of the first tank frame and are summarized in Table 5. For the remainder of the analysis, the highest loads at the tank location were retrieved, corresponding to the configuration with a single aft tank.

A. Design of Experiments (DOE)

With the critical sizing loads determined, a DOE was conducted to identify the most efficient tank topology. The frame height, number of frames and number of stringers were changed between designs. As the hydrogen fuel mass was set as a requirement, the tank must be longer in designs with a higher frame height to accommodate the required fuel. Therefore, it is more appropriate to express the results in terms of tank length, frame pitch and stringer pitch allowing a fair comparison between cases and a clear identification of the design trends.

Figure 13 summarizes the results obtained. It is clearly noticeable that the best designs utilize the minimum tank length, thus minimum frame height, along with the minimum frame and stringer pitch. The results are consistent

Table 5 Structural sizing loads at the aft tank

Load	aft	forward & aft	Unit
External Pressure P	-21.66	-21.66	kPa
1G			
Shear force V_z	168.2	200.8	kN
Bending moment M_y	-1792	-1250	kNm
2.5G			
Shear force V_z	415.9	495.7	kN
Bending moment M_y	-4427	-3077	kNm
Engine out			
Shear force V_z	133.8	155.9	kN
Bending moment M_y	-1393	-890.3	kNm

with the expectations and follow from the design constraints defined earlier. The buckling stability of the skin panels is directly related to the stringer pitch. As the stringer pitch reduces, lower skin thicknesses can be used, as shown in Figure 14a. Similarly, the frame pitch affects the buckling stability of the stringers. Figure 14b illustrates that an increase in frame pitch results in an increase in stringer height.

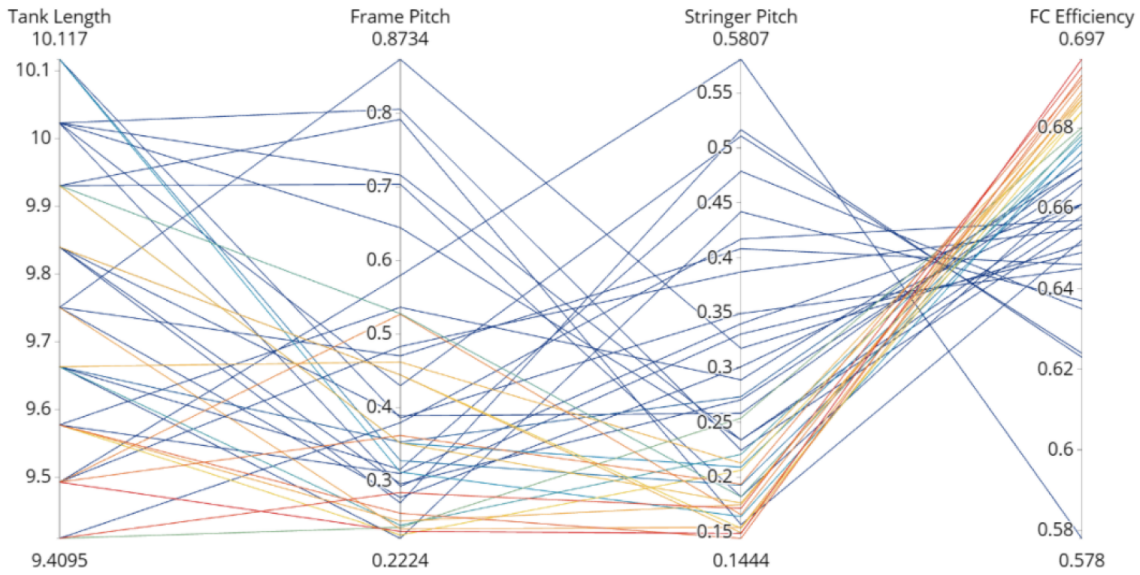

Fig. 13 Parallel coordinate plot of DOE results. Line colors correspond to fuel containment efficiency (rightmost vertical axis)

However, it is also interesting to see that slight increase of frame and stringer pitch above the minimum value have marginal impact on fuel containment efficiency. To illustrate this, Figure 15 shows that the maximum fuel containment efficiency of 70% is obtained for a frame pitch of 250mm and a stringer pitch of 150mm. Another design in the DoE uses roughly twice the frame pitch (536mm) and stringer pitch (286mm) achieves an only 4% lower fuel containment efficiency. Note that the mass of the attachments was included in the allowance of 8% used to estimate the total tank mass. However, this allowance does not account for the number or length of stiffeners. A more realistic estimate and would likely favor designs with fewer stiffeners.

Based on the results obtained, a fixed combination of the studied variables was selected, consisting of 15 frames, 80 stringers and a frame height of 120mm. This was used as a baseline for the remaining analyses.

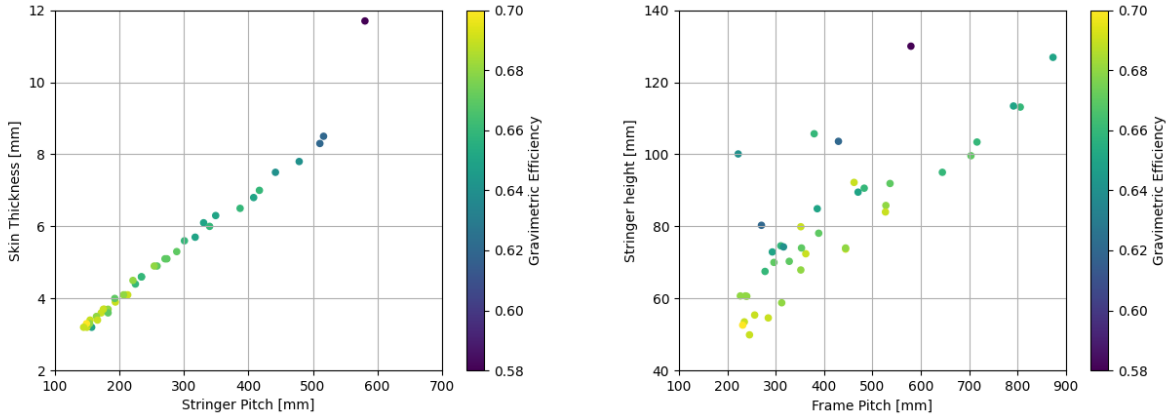

(a) Sensitivity of skin thickness to stringer pitch **(b) Sensitivity of stringer height to frame pitch**

Fig. 14 Initial sensitivity analysis

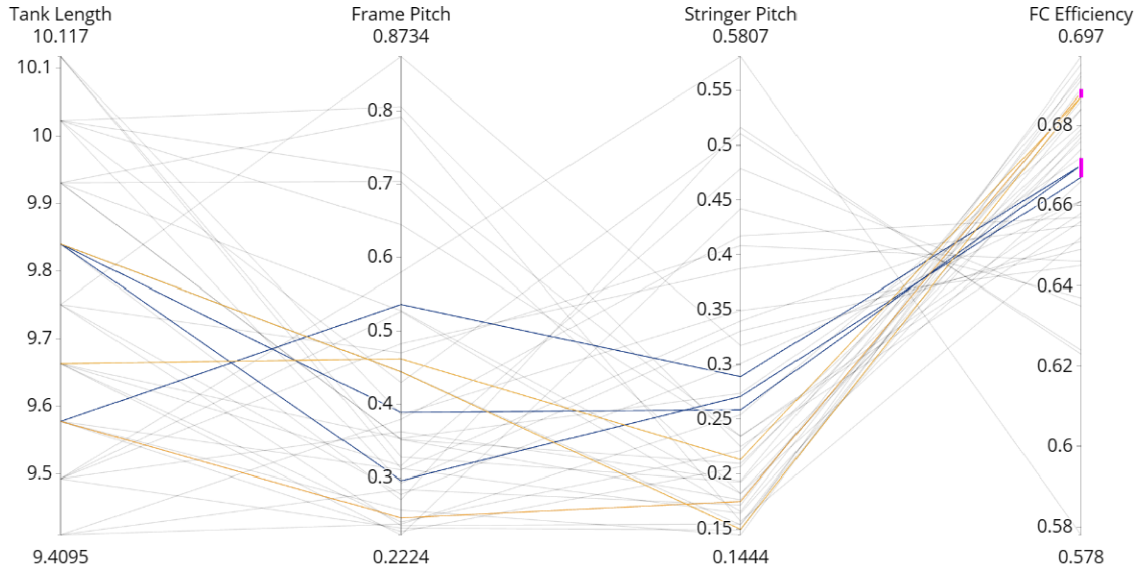

Fig. 15 Parallel coordinate plot of selected DOE results

B. Stringer and dome shape

With the main topology of the tank structure defined, more detailed studies can be carried out. The geometry of the stiffeners was analyzed first, as it influences the behavior of the shell structure under compression. Typically, hat stringers improve the stability of the skin, as they are supported on both sides reducing the unsupported width of the skin. To evaluate if this translates into a mass reduction, a configuration with hat stringers was tested and the results were compared to the previous ones obtained with Z stringers. The results, shown in Table 6, show that the configuration with hat stringers is superior from a gravimetric point of view. It allows lower skin thicknesses, reducing the overall mass of the stiffened wall by 13%, and increasing the FC efficiency by 3 percentage points. The reason is that the hat shape permits the stringers to achieve a larger height without buckling, since they form a closed profile in combination with the skin.

Hence, hat stringers were used for the remainder of the study. It should be noted that additional factors would need to be considered to select the best stringer shape for a given application. For instance, if good corrosion resistance is required, Z-stringers may be selected instead of hat stringers as the latter tend to trap water within their shape and are more difficult to inspect. Attaching hat stringers to the skin also requires a larger amount of fasteners. These

Table 6 Comparison between stiffened shells with Z and hat stringers

Stringer Shape	t_{sk} [mm]	t_{str} [mm]	h_{str} [mm]	$m_{wall_{ex}}$ kg	m_{tank} kg	η_{FC} [0-1]
Z	3.1	1.8	67.7	1047	2467	0.70
Hat	2.1	0.6	88.9	728	2148	0.73

considerations, like the choice to use only a single type and size of stringer, were however out of scope for this study.

The analysis also took into account the impact of changing the shape of the tank domes. The ratio between the the tank radius and the dome length was varied between 1 and 2, with the first corresponding to a spherical dome. Figure 16 shows that, for the same fuel mass, the external wall mass increases as dome length decreases, which is explained by the increase in skin thickness to cope with the increasing frame pitch, as the cylindrical section becomes longer. However, the mass of the inner shell decreases due to the reduction in surface area. As a result, the change in dome shape does not significantly affect the fuel containment efficiency, and other factors must be considered to select the best design. Perhaps the most important parameter is the tank length, which has a direct impact on the fuselage length and passenger capacity. The shortest tank length is obtained with the largest dome factor, theoretically pointing to thee upper bound of the investigated range as the most suitable design. In practice, however, it is expected that a transition radius or a knuckle is used to ease the manufacturing, leading to a conservative selection of a dome factor of 1.6 for the research. Also, Brewer [5] found in his study that this was the shape that would result in the lowest operating cost.

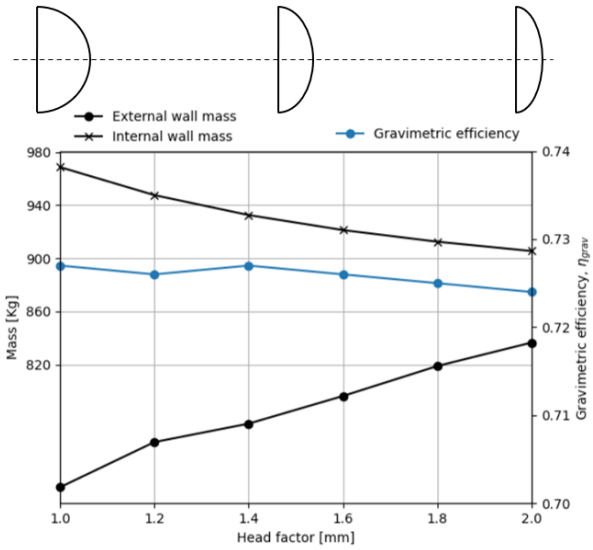

Fig. 16 Sensitivity to dome factor

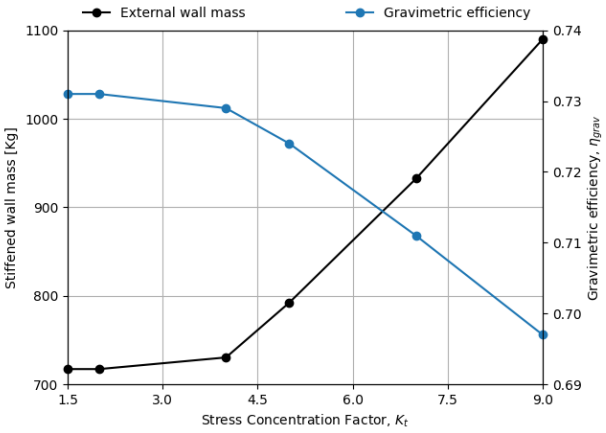

Fig. 17 Sensitivity to stress concentration factor

C. Sensitivity Analysis

In order to increase the confidence on the results, additional sensitivity analyses were carried out on stress concentration factor, the maximum operating pressure (MOP) and the insulation thickness (t_{mli}). Their impact on external wall mass and the tank's fuel containment efficiency are reported in this section.

Figure 17 shows the impact of changing the stress concentration factor (k_t) used in the fatigue constraint (see Equation 10), to decrease the allowable stress. Figure 17 shows that, the fatigue criterion is actively constraining the design. As expected, the mass of the stiffened wall decreases as k_t decreases and fatigue has only mild effects on the design for values of k_t lower than 3. Since this research pertains to preliminary design, a conservative value of 4.5 has been used throughout.

Figure 18 displays the sensitivity of the results to changes in Maximum Operating Pressure (MOP) and insulation thickness. The pressure studied in this case refers to the internal pressure of the liquid hydrogen, which directly affects the sizing of the inner shell, according to Equation 1. Increasing MOP increases the thickness of the inner wall and the

inner wall mass, lowering the fuel containment efficiency of the tank. Therefore, it is desirable to use the lowest possible MOP, while maintaining a safe value above atmospheric pressure avoiding issues with oxygen ingestion. The impact of MOP on the external shell mass is small and only related to the change in tank length due to the change in the internal wall thickness. The thickness of the MLI insulation was considered constant with respect to MOP, which is a reasonable assumption considering its high thermal performance. The impact on the fuel containment efficiency of varying the insulation thickness is less significant than changes in the MOP, as the density of the insulation material is only 1.6% of the density of inner wall material.

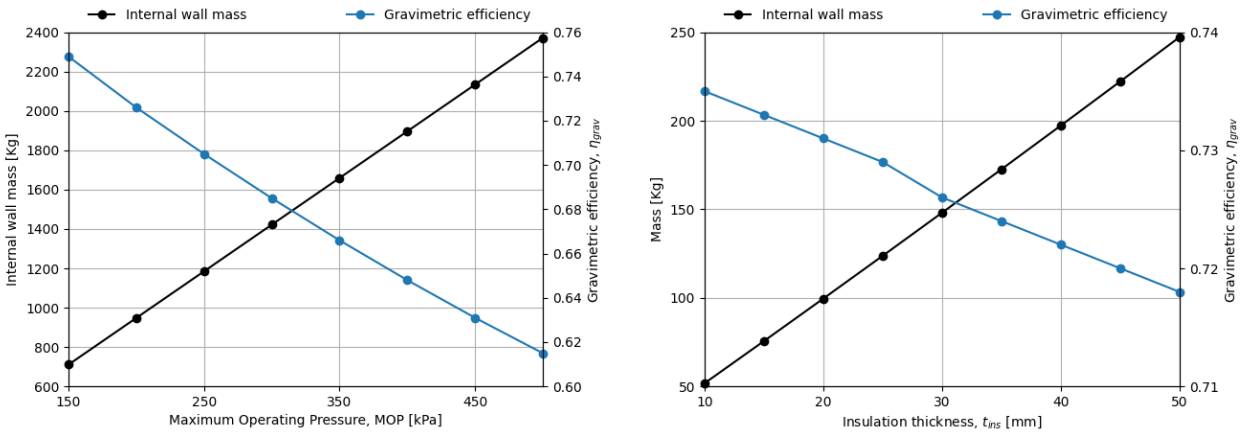

(a) Sensitivity to maximum operating pressure

(b) Sensitivity to insulation thickness

Fig. 18 Results of sensitivity analysis

D. Summary and comparison with literature

In this work, a maximum fuel containment efficiency of 0.71 was obtained for an aft tank integrated into the baseline aircraft, and a fuel containment efficiency of 0.70 for the combination of a forward & aft tank integrated into the same aircraft. The characteristics of both tank designs are shown in Table 7. The results are consistent with existing integral tank designs found in literature. For example, results by Onorato et al. [11] and Silberhorn et al. [4], who also studied aircraft of similar size and range, translate to values of 0.79 and 0.78, respectively, while values reported by Brewer [5] result in 0.76 for a long-range aircraft. For the forward & aft layout, the results by Onorato et al. [11] lead to a value of 0.76. Note that in literature various definitions of gravimetric efficiency are found and it is generally not explicitly clear which elements are included in the tank mass. Hence, a one-to-one comparison is often not possible. Also note that the studies mentioned above regard a single wall design with foam insulation, which explains their slight superiority in fuel containment efficiency. In turn, this means that a more robust double-walled design with MLI insulation may not cause a large increase in tank mass.

VI. Conclusions and Future Work

This research proposes a new integral tank concept to carry liquid hydrogen in the fuselage of commercial aircraft. This concept uses a double wall architecture with outward-facing reinforcements and vacuum insulation, avoiding concerns about the suitability of single-walled designs while providing an efficient thermal insulation. A method was developed to size the external stiffened wall based on a parametric framework, allowing for quick mass estimations of different tanks and an investigation of influences on tank structure mass.

A preliminary analysis of an aft tank for a short/medium range aircraft indicates that fuel containment efficiencies up to 0.71 can be obtained, which is comparable with single-walled integral tank designs. Here, it is important to note that single wall designs are problematic for continued use applications due to: 1. insulation embrittlement, 2. air ingress, 3. insulation thickness (volume constraints), 4. inspectability of the fuselage-load-bearing structure. Additionally, an integral tank integration into the fuselage requires cutouts or openings for cables, piping etc., in a constrained volume. The proposed outward-facing reinforcements allow to pass cables or piping around the tank without changing the fuselage aerolines or affecting the tank shape. The frames on the outer shell connect normally to the aircraft skin, and

**This factor is according to Equation 13, to account for manufacturing tolerances, joints and supports/mounts for fuel-related operating systems.

Table 7 Summary of chosen designs. Note that the forward tank is a non-integral tank and not included in the values below. Only values for the aft tanks in both layouts are reported.

	Aft layout	Forward & aft layout	
Parameter	**Value aft tank**	**Value aft tank**	**Unit**
Fuel mass	5.66	3.21	t
Fuselage radius	1.99	1.99	m
Tank length	8.43	5.14	m
Dome ratio	1.6	1.6	-
Number of stringers	80	80	-
Number of Frames	15	7	-
Inner shell thickness	4.0	4.0	mm
Insulation thickness	30.0	30.0	mm
Outer shell thickness	1.3 (avg)	1.5 (avg)	mm
Fairing thickness	1.6	1.6	mm
Inner shell mass	1.09	0.66	t
Insulation mass	132	80	kg
Outer shell mass	749	387	kg
Fairing mass	93	43	kg
Divider mass	94	94	kg
Manufacturing factor**	1.08	1.08 -	
Total tank mass (m_{tank})	2.29	1.37	t
Fuel containment efficiency (η_{FC})	0.71	0.70	-

do not interfere with the vacuum, thus permitting a very compact insulation using vacuum-assisted materials like MLI and LCI[15] which do not suffer from embrittlement. The double wall protects the insulation from external influences and air ingress, while inspectability of the fuselage integral structure remains possible thanks to the outward-facing frames and stingers.

The study has shown that buckling plays a crucial role in the sizing of the vacuum-insulated tanks. As a result, optimum designs should use low stringer and frame pitch. For the same reason, hat stringers were found to be more efficient than z stringers. The insulation mass has been found to have only a minor influence on the overall tank mass, which also means that an increase in dormancy time beyond the required minimum, or use of redundant insulation layers to insure against degradation of the vacuum are unlikely to cause significant penalties.

The results obtained in this study are encouraging and motivate further work on this tank concept. Future work should focus on the suspension design between the inner and outer walls, as well as the load-cases this may introduce, and include crash worthiness. The research could also be extended to include conical tanks in different locations in the aircraft. A further point of investigation is the impact on the aircraft design within a closed design loop, as well as a comparison to a double-walled non-integral tank, both in terms of structure mass as well as practical aspects like inspection, maintenance and repair.

Acknowledgments

The authors would like to thank Dr. Saullo Castro for his feedback on the structural design and his invaluable inputs regarding the FEM modeling. This article is based on the work performed during the MSc. thesis of Tomas Montellano [37].

References

[1] Lee, D. S., Fahey, D. W., Skowron, A., Allen, M. R., Burkhardt, U., Chen, Q., Doherty, S. J., Freeman, S., Forster, P. M., Fuglestvedt, J., et al., "The contribution of global aviation to anthropogenic climate forcing for 2000 to 2018," *Atmospheric Environment*, Vol. 244, 2021, p. 117834.

[2] Rao, A. G., Yin, F., and Werij, H. G., "Energy transition in aviation: The role of cryogenic fuels," *Aerospace*, Vol. 7, No. 12, 2020, p. 181.
[3] Fuel Cells and Hydrogen 2 Joint Undertaking, "Hydrogen-powered aviation – A fact-based study of hydrogen technology, economics, and climate impact by 2050," Tech. rep., Publications Office of the European Union, 2020. https://doi.org/doi/10.2843/471510.
[4] Silberhorn, D., Atanasov, G., Walther, J.-N., and Zill, T., "Assessment of Hydrogen Fuel Tank Integration at Aircraft Level," *Deutscher Luft- und Raumfahrtkongress 2019*, 2019, pp. –.
[5] Brewer, G. D., *Hydrogen Aircraft Technology*, CRC Press, Boca Raton, 1991.
[6] Verstraete, D., "The Potential of Liquid Hydrogen for long range aircraft propulsion," Ph.D. thesis, Cranfield University, 2009.
[7] Winnefeld, C., Kadyk, T., Bensmann, B., Krewer, U., and Hanke-Rauschenbach, R., "Modelling and designing cryogenic hydrogen tanks for future aircraft applications," *Energies*, Vol. 11, No. 1, 2018, p. 105.
[8] Mantzaroudis, V. K., and Theotokoglou, E. E., "Computational Analysis of Liquid Hydrogen Storage Tanks for Aircraft Applications," *Materials*, Vol. 16, No. 6, 2023, p. 2245.
[9] Huete, J., and Pilidis, P., "Parametric study on tank integration for hydrogen civil aviation propulsion," *International Journal of Hydrogen Energy*, Vol. 46, No. 74, 2021, pp. 37049–37062.
[10] Onorato, G., "Fuel Tank Integration for Hydrogen Airliners," Master's thesis, Delft University of Technology, 2021.
[11] Onorato, G., Proesmans, P., and Hoogreef, M. F. M., "Assessment of hydrogen transport aircraft," *CEAS Aeronautical Journal*, Vol. 13, No. 4, 2022, pp. 813–845. https://doi.org/10.1007/s13272-022-00601-6.
[12] van Woensel, C., "Integration of a Liquid Hydrogen Fuel Tank into the Concept of the Flying-V," Master's thesis, Delft University of Technology, 2021.
[13] Brewer, G., "Advanced supersonic technology concept study: Hydrogen fueled configuration," Tech. Rep. NASA-CR-114718, NASA, 1974.
[14] Gomez, A., and Smith, H., "Liquid hydrogen fuel tanks for commercial aviation: Structural sizing and stress analysis," *Aerospace Science and Technology*, Vol. 95, 2019, p. 105438. https://doi.org/https://doi.org/10.1016/j.ast.2019.105438.
[15] Fesmire, J. E., Augustynowicz, S. D., and Scholtens, B. E., "Robust Multilayer Insulation For Cryogenic Systems," *AIP Conference Proceedings*, Vol. 985, No. 1, 2008, p. 1359–1366. https://doi.org/10.1063/1.2908494, URL https://aip.scitation.org/doi/abs/10.1063/1.2908494.
[16] Brewer, G. D., Morris, R. E., Lange, R. H., and Moore, J. W., "Study of the application of hydrogen fuel to long-range subsonic transport aircraft, volume 2," Tech. Rep. NASA-CR-132559, NASA, 1975.
[17] Wu, S., Li, J., Ding, P., and Ouyang, Z., "Calculation and analysis of optimal layer density for variable density multilayer insulation based on layer by layer model and Lockheed equation," *Cryogenics*, 2023, p. 103699.
[18] Johnson, W., "Thermal analysis of low layer density multilayer insulation test results," *AIP Conference Proceedings*, American Institute of Physics, 2012, pp. 1519–1526.
[19] *Standard Guide for Evacuated Reflective Insulation In Cryogenic Service*, ASTM International, 2019. https://doi.org/10.1520/C0740_C0740M-13, URL https://www.astm.org/c0740_c0740m-13.html.
[20] Johnson, T. F., Weiser, E. S., Grimsley, B. W., and Jensen, B. J., "Cryopumping in cryogenic insulations for a reusable launch vehicle," Tech. rep., NASA, 2003.
[21] Mital, S. K., Gyekenyesi, J. Z., Arnold, S. M., Sullivan, R. M., Manderscheid, J. M., and Murthy, P. L., "Review of current state of the art and key design issues with potential solutions for liquid hydrogen cryogenic storage tank structures for aircraft applications," Tech. Rep. NASA/TM-2006-214346, NASA, 2006.
[22] Verstraete, D., Hendrick, P., Pilidis, P., and Ramsden, K., "Hydrogen fuel tanks for subsonic transport aircraft," *International journal of hydrogen energy*, Vol. 35, No. 20, 2010, pp. 11085–11098.
[23] Al-Rubaie, K., "A general model for stress-life fatigue prediction," *Materialwissenschaft und Werkstofftechnik: Entwicklung, Fertigung, Prüfung, Eigenschaften und Anwendungen technischer Werkstoffe*, Vol. 39, No. 6, 2008, pp. 400–406.
[24] Torenbeek, E., *Synthesis of Subsonic Airplane Design*, Delft Univ. Press, Delft, The Netherlands, 1982.
[25] Klug, H., and Faass, R., "CRYOPLANE: hydrogen fuelled aircraft — status and challenges," *Air & Space Europe*, Vol. 3, 2001, pp. 252–254. https://doi.org/10.1016/S1290-0958(01)90110-8.
[26] Heidebrecht, A., Burger, K., Hoogreef, M., Vos, R., Isikveren, A. T., and Rao, A. G., "Development of a Hydrogen-powered Fuselage-mounted BLI Propulsor Add-on for Passenger Aircraft," *33rd congress of international council of the aeronautical sciences, Stockholm, Sweden*, 2022, pp. 4–9.
[27] Megson, T. H. G., *Aircraft structures for engineering students*, Butterworth-Heinemann, 2016.
[28] Lomax, T. L., *Structural loads analysis for commercial transport aircraft: theory and practice*, American Institute of Aeronautics and Astronautics, 1996.
[29] Şen, I., "Aircraft Fuselage Design Study," Master's thesis, Delft University of Technology, 2010.
[30] Parello, R., Gourinat, Y., Benard, E., and Defoort, S., "Structural sizing of a hydrogen tank for a commercial aircraft," *Journal of Physics: Conference Series*, IOP Publishing, 2024, pp. 12–40.
[31] Klarholm, D., "Offset modeling of shell elements: a study in shell element modeling using Nastran," Master's thesis, Linköping University, 2016.
[32] Krakers, L. A., "Parametric fuselage design: Integration of mechanics and acoustic & thermal insulation," Ph.D. thesis, Delft University of Technology, 2009.
[33] Nanninga, M., "High-Fidelity Structural Sizing Method for Weight Estimation of a Flying-V," Master's thesis, Delft University of Technology, 2023.
[34] De Jong, J., Schütz, D., Lowak, H., and Schijve, J., "A standardized load sequence for flight simulation tests on transport aircraft wing structures," *NLR-TR 73029 U, LBF Bericht FB-106*, 1973.
[35] Turrel, N., and Auriche, D., "Widespread fatigue damage-A300B: compliance with ageing aircraft regulation," *Airbus Fast Magazine*, Vol. 51, 2013, pp. 17–23.
[36] Huete, J., Nalianda, D., and Pilidis, P., "Impact of tank gravimetric efficiency on propulsion system integration for a first-generation hydrogen civil airliner," *The Aeronautical Journal*, Vol. 126, No. 1302, 2022, pp. 1324–1332.
[37] Oom Ortiz de Montellano, T., "Structural Analysis of a New Integral Tank Concept for Hydrogen Storage On-board Commercial Aircraft," Master's thesis, TU Delft, 2024. https://resolver.tudelft.nl/uuid:8ab68eb3-77dc-4acf-9768-6b379b8ef24d.